Journal of Alloys and Compounds 639 (2015) 593–601

Contents lists available at ScienceDirect

Journal of Alloys and Compounds

journal homepage: www.elsevier.com/locate/jalcom

Experimental study of the phase equilibria in the Mg–Zn–Ag ternary system at 300 °C

Jian Wang [a,*], Yi-Nan Zhang [b], Pierre Hudon [c], In-Ho Jung [c], Mamoun Medraj [b,d], Patrice Chartrand [a]

[a] Center for Research in Computational Thermochemistry (CRCT), Department of Chemical Engineering, École Polytechnique, Montréal, Québec H3C 3A7, Canada
[b] Department of Mechanical Engineering, Concordia University, 1455 De Maisonneuve Blvd. West, Montreal, Quebec H3G 1M8, Canada
[c] Department of Mining and Materials Engineering, McGill University, 3610 University Street, Montreal, Quebec H3A 0C5, Canada
[d] Department of Mechanical and Materials Engineering, Masdar Institute, Masdar City, P.O. Box 54224, Abu Dhabi, United Arab Emirates

ARTICLE INFO

Article history:
Received 27 February 2015
Received in revised form 24 March 2015
Accepted 25 March 2015
Available online 2 April 2015

Keywords:
Mg–Zn–Ag
Phase diagram
Diffusion couple
X-ray
SEM
EDS

ABSTRACT

The phase equilibria in the Mg–Zn–Ag ternary system at 300 °C were investigated using three diffusion couples and 35 key samples. Scanning electron microscopy (SEM) equipped with energy-dispersive spectroscope (EDS) and X-ray diffraction (XRD) techniques were used for homogeneity ranges and crystal structure determination. Large solid solubility limits, due to substitution among Mg, Zn and Ag atoms in Mg_3Ag and $MgZn_2$ phases, were observed in the present work. Solid solubility limits of Ag and Zn in the hcp (Mg) phase were found to be less than 1 at.%. The extended solid solubilities of the $Mg_{12}Zn_{13}$, Mg_2Zn_3, $MgZn_2$ (C14), Mg_2Zn_{11}, Ag_5Zn_8 and hcp ($AgZn_3$) sub-binary compounds were also determined in the Mg–Zn–Ag ternary system. In addition, a bcc continuous ternary solid solution forms between MgAg (bcc_B2) and AgZn (bcc_A2) at 300 °C.

1. Introduction

The automotive and aeronautic industries have an increasing interest in magnesium based alloys. This is due to their low density, compared with aluminum and steel; thus vehicle weight and fuel consumption can be reduced. Since the Mg–Al based alloys, which are most widely used, have poor mechanical properties (such as yield and tensile strength, hardness, etc) at elevated temperature up to 200 °C or higher, their applications are limited. Consequently, many new Mg alloys are under development for high temperature applications. The effect of Ag on Mg-based alloys has been recently widely investigated. Ag significantly enhances the grain refinement, hardness of Mg-based alloys [1–4]. Ben-Hamu et al. [1] found that addition of Ag (about 1–3 at.%) leads to better grain refining and increase in hardness. But unfortunately, the corrosion resistance of these alloys is reduced. Park et al. [5] reported that the addition of Ag into Mg–Zn alloys can increase the tensile strength in a double aging treatment. Since Ag acts as an important micro-alloying element for Mg–Zn based alloys, a comprehensive understanding of the phase equilibria in the Mg–Zn–Ag ternary system, especially in the Mg-rich region, is of primary importance in Mg-based alloys development.

The phase diagrams of the three binary sub-systems Mg–Zn [6–9], Mg–Ag [10–13] and Zn–Ag [14–21] of the Mg–Zn–Ag ternary system have been well investigated using experimental and thermodynamic modeling methods. The final accepted version of each binary phase diagram [9,10,14,15] is shown in Fig. 1. The phase diagram of the Mg–Zn binary system has five intermetallic compounds: Mg_2Zn_{11}, $MgZn_2$ (C14), Mg_2Zn_3, $Mg_{12}Zn_{13}$ and $Mg_{51}Zn_{20}$, and two terminal solid solutions, hcp (Mg) and hcp (Zn). It is worth noting that $Mg_{51}Zn_{20}$, with minimum solid solubility, is stable only between 325 and 342 °C [22]. The Ag–Mg system was critically reviewed by Nayeb-Hashemi and Clark [13]. There are five solid phases in the Ag–Mg binary system: fcc (Ag), hcp (Mg), MgAg (bcc_B2), $MgAg_3$ (fcc_$L1_2$) and Mg_3Ag. Later, an X-ray diffraction analysis by Prokofev et al. [23] demonstrated that Mg_3Ag appears to be constituted of ε, Body centered tetragonal (bct), at low temperature and ε′, face center cubic (fcc), at high temperature. The structural formula of ε′ (fcc) is $Ag_{17}Mg_{54}$ with a stable temperature range of 465–494 °C [23]. Kolesnichenko et al. [11] revised the formula for previously reported Mg_3Ag to Mg_4Ag; Kreiner and Spiekermann [24] recently re-investigated ε (Mg_3Ag), and reported that it has an fcc crystal structure with space group $Fm\bar{3}$ and formula $Mg_{25.04}Ag_{7.96}$ (designated Mg_3Ag in the present study). Lim et al. [12] and Wang et al. [10] modeled

* Corresponding author at: Centre de Recherche en Calcul Thermochimique (CRCT), École Polytechnique de Montréal, Montréal, QC H3C 3A7, Canada. Tel.: +1 5143404711x2483; fax: +1 514 3405840.
E-mail address: jian.wang@polymtl.ca (J. Wang).

http://dx.doi.org/10.1016/j.jallcom.2015.03.195
0925-8388/

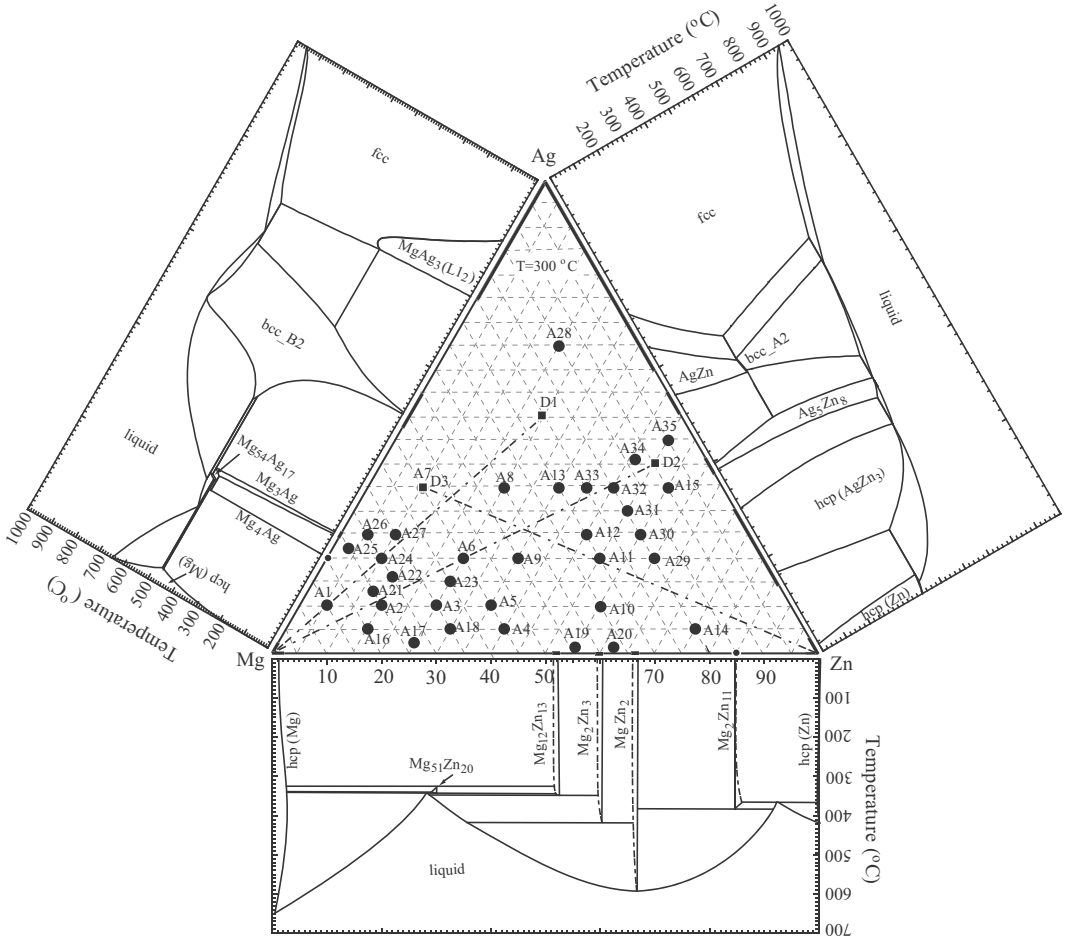

Fig. 1. Binary phase diagram constituting the Mg–Zn–Ag ternary system with the compositions of diffusion couple and key alloys designed in the present work.

the phase equilibria of the Mg–Ag binary system using the calculation phase diagram (CALPHAD) method. The final accepted phase diagram of the Mg–Ag binary system includes fcc (Ag), $MgAg_3$ ($L1_2$), hcp (Mg), bcc_B2, Mg_3Ag ($Mg_{25.04}Ag_{7.96}$), $Mg_{54}Ag_{17}$ and Mg_4Ag ($Mg_{37}Ag_9$). Heycock and Neville [25], Petrenko et al. [17,18], Owen and Edmunds [19–21] and Andrews et al. [16] studied the phase equilibria and liquidus of the Ag–Zn binary system experimentally. The phase diagram of the Ag–Zn binary system was optimized by the CALPHAD technique by Gomez-Acebo [15] and Wang et al. [14]. The phase diagram of this binary system includes fcc (Ag), β (bcc_A2), γ (Ag_5Zn_8), ζ (AgZn), ε (hcp_$AgZn_3$) and hcp (Zn) phases. All the solid phases and their crystal structure information in the binary sub-systems of the Mg–Zn–Ag ternary system are summarized in Table 1.

To date, limited experimental results have been reported on the phase equilibria of the Mg–Zn–Ag ternary system [26–28]. Raynor and Smith [26] reported isothermal sections of the Mg–Zn–Ag ternary system in the Ag-rich region (50–100 at.% Ag) at 250, 450 and 650 °C. The bcc solid solution between AgZn (bcc_A2) and MgAg (bcc_B2) forms a continuous solid solution in these isothermal sections. Matsuo et al. [27,28] reported the isopleth section of Ag50Zn50–Mg50Zn50 and no new ternary phase was observed. As a result, it is essential to investigate thoroughly the phase equilibria in the Mg–Zn–Ag ternary system, especially in the Mg-rich region, for the purposes of Mg–Zn based alloys development.

The aim of the present work is to study experimentally the isothermal section of the Mg–Zn–Ag ternary system at 300 °C with a combined approach involving the diffusion couple technique and the classical equilibrated alloys method. This temperature was chosen because it corresponds to the temperature at which heat treatment is usually performed on Mg based alloys. This work is

Table 1
Crystallography information of the solid phases in the Mg–Zn–Ag ternary system.

System	Phase	Pearson symbol	Strukturbericht designation	Space group	Prototype
Mg–Zn	hcp (Mg)	*hP2*	A3	$P6_3/mmc$	Mg
	hcp (Zn)	*hP2*	A3	$P6_3/mmc$	Mg
	$Mg_{12}Zn_{13}$	–	–	–	–
	Mg_2Zn_3	*mC110*	–	$B2/m$	–
	$MgZn_2$	*hP12*	C14	$P6_3/mmc$	$MgZn_2$
	Mg_2Zn_{11}	*cP39*	$D8_c$	$Pm\bar{3}$	Mg_2Zn_{11}
	$Mg_{51}Zn_{20}$	*oI142*	$D7_b$	*Immm*	$Os_{17}Hf_{54}$
Mg–Ag	hcp (Mg)	*hP2*	A3	$P6_3/mmc$	Mg
	bcc_B2	*cP2*	B2	$Pm\bar{3}m$	CsCl
	fcc (Ag)	*cF4*	A1	$Fm\bar{3}m$	Cu
	$MgAg_3$	*cP4*	$L1_2$	$Pm\bar{3}m$	$AuCu_3$
	Mg_4Ag	*hP92*	–	$P6_3$	Ag_9Mg_{37}
	$Mg_{54}Ag_{17}$	*oI142*	–	*Immm*	$Mg_{54}Ag_{17}$
	Mg_3Ag	*cF264*	–	$Fm\bar{3}$	$Mg_{26}Ag_7$
Zn–Ag	fcc (Ag)	*cF4*	A1	$Fm\bar{3}m$	Cu
	hcp (Zn)	*hP2*	A3	$P6_3/mmc$	Mg
	bcc_A2	*cI2*	A2	$Im\bar{3}m$	W
	AgZn	–	–	–	–
	hcp ($AgZn_3$)	*hP2*	A3	$P6_3/mmc$	Mg
	hcp(Zn)	*hP2*	A3	$P6_3/mmc$	Mg
	Ag_5Zn_8	*cI52*	$D8_2$	$I\bar{4}3m$	Cu_5Zn_8

Table 2
Equilibria compositions obtained from the Mg–Zn–Ag diffusion couples.

Diffusion couples	Phase equilibria	Composition determined by EDS (at.%)								
	Phase 1/phase 2/phase 3	Phase 1			Phase 2			Phase 3		
		Ag	Mg	Zn	Ag	Mg	Zn	Ag	Mg	Zn
D1 (Mg-Mg25Zn25Ag50)	bcc/Mg_3Ag/–	44.4	50.4	5.2	22.3	68.7	9.0	–	–	–
	Mg_3Ag/hcp(Mg)/–	17.0	73.9	9.1	0.3	99.2	0.5	–	–	–
D2 (Mg-Mg10Zn50Ag40)	$MgZn_2$/Ag_5Zn_8/–	25.7	29.5	44.8	38.0	12.1	49.9	–	–	–
	$MgZn_2$/Mg_3Ag/–	6.2	37.6	56.2	12.2	67.9	19.9	–	–	–
	Mg_3Ag/hcp(Mg)/–	5.8	71.1	23.1	0.2	98.0	1.9	–	–	–
D3 (Zn-Mg55Zn10Ag35)	bcc/Mg_3Ag/–	23.5	70.1	6.4	46.4	50.2	3.4	–	–	–
	Mg_3Ag/$MgZn_2$/bcc	21.7	64.8	13.5	15.8	35.1	49.1	44.6	48.8	6.6
	$MgZn_2$/hcp($AgZn_3$)/–	9.5	30.2	60.3	16.2	0.7	83.1	–	–	–

Table 3
Equilibria compositions obtained from the Mg–Zn–Ag key samples.

Sample no.	Alloy nominal composition (at.%)	Phase equilibria	Composition determined by EDS (at.%)								
		Phase 1/phase 2/phase 3	Phase 1			Phase 2			Phase 3		
			Ag	Mg	Zn	Ag	Mg	Zn	Ag	Mg	Zn
A1	Mg85Zn5Ag10	hcp(Mg)/Mg_3Ag/–	0.5	99.0	0.5	17.6	74.5	7.9	–	–	–
A2	Mg75Zn15Ag10	hcp(Mg)/Mg_3Ag/–	0.2	98.5	1.3	12.1	72.4	15.5	–	–	–
A3	Mg65Zn25Ag10	Mg_3Ag/$MgZn_2$/–	12.1	67.3	20.6	5.7	36.8	57.5	–	–	–
A4	Mg55Zn40Ag5	Mg_3Ag/$MgZn_2$/–	7.5	68.0	24.5	2.8	37.7	59.5	–	–	–
A5	Mg55Zn35Ag10	Mg_3Ag/$MgZn_2$/–	13.6	66.5	19.9	7.2	37.1	55.7	–	–	–
A6	Mg55Zn25Ag20	Mg_3Ag/$MgZn_2$/bcc	20.4	63.5	16.1	14.7	37.4	47.9	42.0	50.4	7.6
A7	Mg55Zn10Ag35	Mg_3Ag /bcc/–	20.8	66.1	13.1	42.9	50.8	6.3	–	–	–
A8	Mg40Zn25Ag35	$MgZn_2$/bcc/–	25.9	32.6	41.5	47.7	47.3	5.0	–	–	–
A9	Mg45Zn35Ag20	Mg_3Ag/$MgZn_2$/bcc	19.9	64.2	15.9	14.9	37.3	47.8	41.9	50.4	7.7
A10	Mg35Zn55Ag10	$MgZn_2$/–/–	10.2	35.1	54.7	–	–	–	–	–	–
A11	Mg30Zn50Ag20	$MgZn_2$/–/–	20.1	31.7	48.2	–	–	–	–	–	–
A12	Mg30Zn45Ag25	$MgZn_2$/bcc/–	28.1	30.9	41.0	51.1	37.6	11.3	–	–	–
A13	Mg30Zn35Ag35	$MgZn_2$/bcc/–	28.7	29.9	41.4	50.6	31.0	18.4	–	–	–
A14	Mg20Zn75Ag5	$MgZn_2$/Mg_2Zn_{11}/hcp($AgZn_3$)	6.3	31.3	62.4	2.7	15.1	82.2	13.6	0.8	85.7
A15	Mg10Zn55Ag35	Ag_5Zn_8/–/–	37.6	10.2	52.2	–	–	–	–	–	–
A16	Mg80Zn15Ag5	hcp(Mg)/Mg_3Ag/–	7.7	72.3	20.0	0.7	96.4	2.9	–	–	–
A17	Mg73Zn25Ag2	hcp(Mg)//Mg_3Ag/–	0.2	97.4	2.4	2.4	72.0	25.6	–	–	–
A18	Mg65Zn30Ag5	Mg_3Ag/$MgZn_2$/–	5.8	70.4	23.8	2.1	40.1	57.8	–	–	–
A19	Mg44Zn55Ag1	Mg_3Ag/$Mg_{12}Zn_{13}$/$MgZn_2$	4.2	71.4	24.4	1.1	49.5	49.4	1.6	42.1	56.3
A20	Mg37Zn62Ag1	Mg_2Zn_3/–/–	1.4	39.5	59.1	–	–	–	–	–	–
A21	Mg75Zn12Ag13	hcp(Mg)//Mg_3Ag/–	0.8	97.9	1.30	14.5	74.1	11.4	–	–	–
A22	Mg70Zn14Ag16	Mg_3Ag/–/–	16.0	71	13.0	–	–	–	–	–	–
A23	Mg60Zn25Ag15	Mg_3Ag/$MgZn_2$/–	16.4	67.3	16.3	12.0	38.6	49.4	–	–	–
A24	Mg70Zn10Ag20	Mg_3Ag/bcc/–	21.8	73.0	5.2	42.9	53.9	3.2	–	–	–
A25	Mg75Zn3Ag22	Mg_3Ag/bcc/–	22.2	74.5	3.3	44.0	54.3	1.7	–	–	–
A26	Mg70Zn5Ag25	Mg_3Ag/bcc/–	20.7	70.7	8.6	42.2	52.5	5.3	–	–	–
A27	Mg65Zn10Ag25	Mg_3Ag/bcc/–	41.9	51.9	6.2	20.4	68.6	11.0	–	–	–
A28	Mg15Zn20Ag65	bcc_A2/fcc/–	54.3	20.3	25.4	63.4	15.9	20.8	–	–	–
A29	Mg20Zn60Ag20	$MgZn_2$/hcp($AgZn_3$)/–	15.8	31.6	52.6	20.0	2.5	76.5	–	–	–
A30	Mg20Zn55Ag25	$MgZn_2$/Ag_5Zn_8/hcp($AgZn_3$)	24.6	30.5	44.9	35.3	9.7	55.0	27.9	2.9	69.2
A31	Mg20Zn50Ag30	$MgZn_2$/Ag_5Zn_8/hcp($AgZn_3$)	24.5	29.3	46.2	35.5	8.7	55.8	28.4	3.2	68.4
A32	Mg20Zn45Ag35	$MgZn_2$/Ag_5Zn_8/–	26.2	29.9	43.9	36.5	11.6	51.9	–	–	–
A33	Mg25Zn40Ag35	$MgZn_2$/bcc/–	28.0	29.9	42.1	49.8	25.6	24.6	–	–	–
A34	Mg13Zn46Ag41	$MgZn_2$/Ag_5Zn_8/–	29.1	29.8	41.1	39.0	15.4	45.6	–	–	–
A35	Mg5Zn50Ag45	Ag_5Zn_8/bcc/–	40.4	4.3	55.3	49.6	6.8	43.6	–	–	–

part of a comprehensive research program to develop a thermodynamic database of Mg–X (X: Ag, Ca, In, Li, Na, Sn, Sr, Zn) based alloys for automotive applications [8,10,29,30–35].

2. Experimental procedure

Three solid-state diffusion couples and 35 ternary key samples of the Mg–Zn–Ag ternary system were prepared using pure Mg (99.8 wt.%), Zn (99.5 wt.%), and Ag (99.95 wt.%) obtained from Alfa Aesar in USA. The prepared metal pieces were then melted in an induction furnace under high purity argon atmosphere. The nominal compositions for the end members of the diffusion couples and other key alloys are plotted in Fig. 1 and listed in Tables 2 and 3. In order to minimize the interaction of the samples with the crucibles, Ta cubic-shaped crucibles were made using Ta foil (99.5 wt.% purity, 0.15 mm thickness). Each alloy was re-melted three times in its crucible to obtain a homogeneous alloy. The maximum evaporation loss was less than 3 wt.%. To prepare solid state diffusion couples, the contacting surfaces of the alloy pieces were ground with 1200 grit SiC paper and polished using a 1 μm water-based diamond suspension with 99% pure ethanol as lubricant. Two end-members were gently pressed and further clamped with a steel ring. Diffusion couples and key alloys were then placed in a Ta container and sealed into quartz capsules under argon to avoid oxidation of Mg. Diffusion couples and key alloys were annealed at 300 °C for 21 and 35 days, respectively. It was necessary to anneal the key alloys longer than the diffusion couples to obtain fully equilibrated samples. Quenching was carried out in water without breaking the quartz tube, to avoid reaction of the sample with water. Phase relationships and constitutions of the diffusion couples and key alloys were determined using scanning electron microscopy (SEM) equipped with energy-dispersive spectroscopy (EDS). Analyses of the Mg–Zn–Ag samples were effected with a HITACHI S-3400N using an accelerating voltage of 15 kV, a spot size of 3 μm, and counting times of 60 s. Five points in different areas of each phase were measured and averaged to obtain the phase compositions. The accuracy of EDS measurement is about ±1 at.%. It should be noted that values indicated less than 1 at.% obtained in the present work are in low accuracy quality. But these values still are very worthy to be stated as references showing the extremely limits of solid solubility.

Crystal structures of the phases present in the annealed samples were identified by X-ray diffraction (XRD). XRD patterns were obtained with the PANanalytical X'pert Pro powder X-ray diffractometer using Cu Kα radiation at 45 kV and

40 mA. The spectra were acquired from 20° to 90° (2θ) with a 0.02° step size. The collected patterns were analyzed with the X'Pert HighScore plus Rietveld analysis software in combination with Pearson's crystal database [36]. Si was used as an internal calibration standard to enable correction of the zero shift and specimen surface displacement which are the most serious systematic errors in X-ray powder diffraction patterns.

3. Results and discussion

3.1. Diffusion couples results

In order to obtain general information on the equilibrium phase relationships in the Mg–Zn–Ag ternary system at 300 °C, three diffusion couples, D1 (Mg-Mg25Zn25Ag50), D2 (Mg-Mg10Zn50Ag40) and D3 (Zn-Mg55Zn10Ag35), were prepared in the present work.

Backscatter electron (BSE) images of diffusion couple D1, with gradually increased magnification of the area of interest, are shown in Fig. 2. During the heat treatment, extensive inter-diffusion of Ag, Mg and Zn took place, allowing various equilibrated phases to form. Four continuous diffusion layers were observed clearly in the diffusion couple D1, as shown in Fig. 2a. Phase composition analysis was carried out with EDS. Four phases with continuous layers, viz., bcc_A2, bcc_B2, Mg_3Ag, and hcp (Mg) were formed in the diffusion couple D1. It should be noted that the boundary of order–disorder (B2/A2) transformation of the bcc phase was not able to be determined in the present work using SEM/EDS analysis. However, according to the two different phase layers observed in D1, as shown in Fig. 2, we propose that the compositions obtained with MgAg-rich alloys are bcc_B2, and the remaining region of this continuous solution is bcc_A2. The B2/A2 order–disorder transformation boundary also was proposed, as inferred by the authors. Moreover, further experiment was needed to verify the boundary of B2/A2 or even second-order transformation as B2/$D0_3$ or A2/$D0_3$ phase transformation of the bcc continuous solution in the Mg–Zn–Ag system. Between the bcc_A2 and bcc_B2 phases, the discontinuous diffusion layer of the $MgZn_2$ (C14) phase was observed as shown in Fig. 2b. This phenomenon may be explained in two ways: (i) Mg has a high diffusion coefficient, which leads to the formation of the bcc phase with the Mg25Zn25Ag50 end-member first. Heat treatment time is not enough to form a continuous equilibrium layer of $MgZn_2$ (C14) between the phases of bcc_A2 and bcc_B2. Hence the diffusion path should be through bcc_A2 ↔ $MgZn_2$ (C14) ↔ bcc_B2. (ii) The diffusion path can also go through the three-phase region of bcc_B2 + $MgZn_2$ (C14) + bcc_A2, where $MgZn_2$ served as a precipitated compound at the interface of bcc_B2 and bcc_A2 to form a three-phase equilibrium. A similar phenomenon was found also in our previous work [34]. By taking advantage of the local equilibrium at the interfaces formed between the phases, the sequence of the phases formed and diffusion path in the D1 could be deemed to be bcc_A2 ↔ $MgZn_2$ (C14) ↔ bcc_B2 ↔ Mg_3Ag ↔ hcp (Mg). The EDS scanning line was used to determine the solid solubility of the phases formed as shown in Fig. 2c. As shown in Fig. 2c, a solubility range of 17–22 at.% Ag, with constant 9 at.% Zn in Mg_3Ag, was observed (Fig. 2c). This indicates that solid solubility in Mg_3Ag formed a substitutional solid solution, where Ag substitutes for

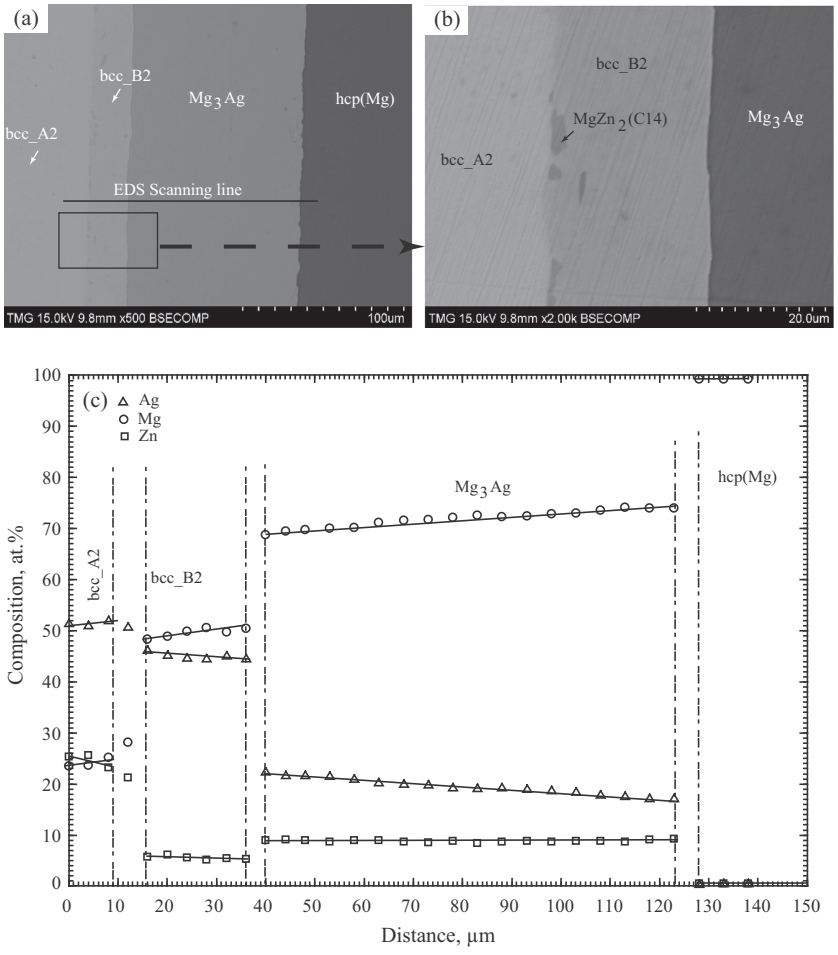

Fig. 2. Backscatter electron (BSE) images of diffusion couple D1 with gradually increased magnification of the area of interest: (a) diffusion layers obtained in diffusion couple D1, (b) gradually increased magnification of the area interest, (c) solid solubility of the phases determined using DSC scan line.

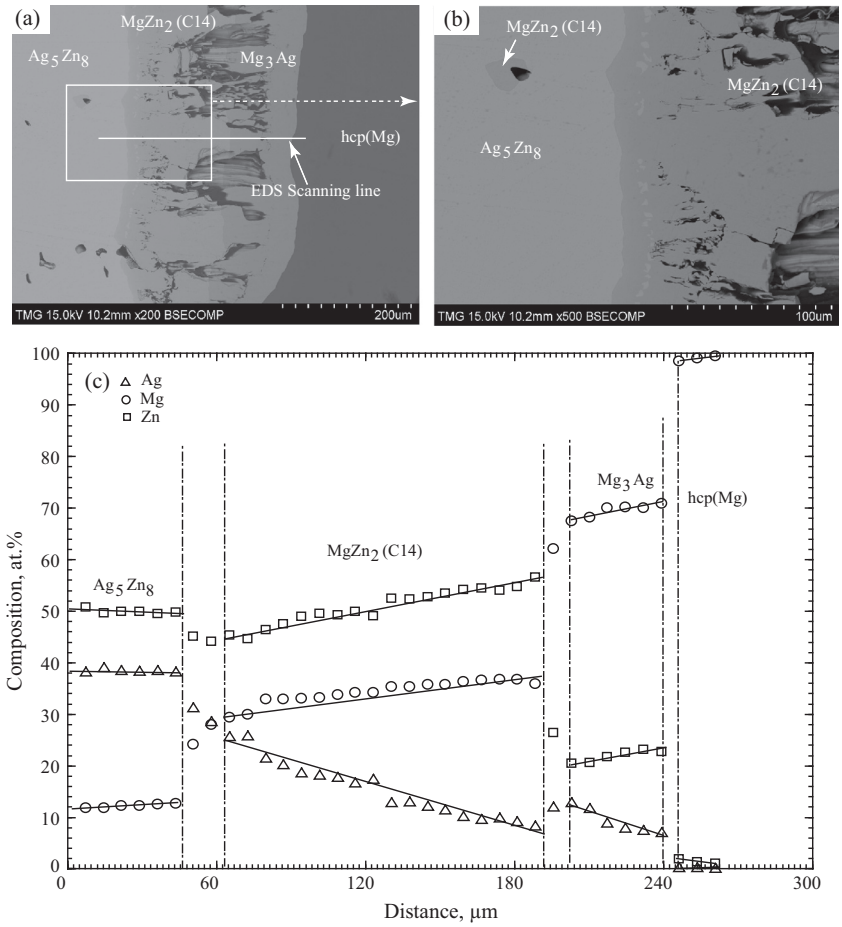

Fig. 3. BSE images of diffusion couple D2 with gradually increased magnification of the area of interest: (a) diffusion layers obtained in diffusion couple D2, (b) gradually increased magnification of the area interest, (c) solid solubility of the phases determined using DSC scan line.

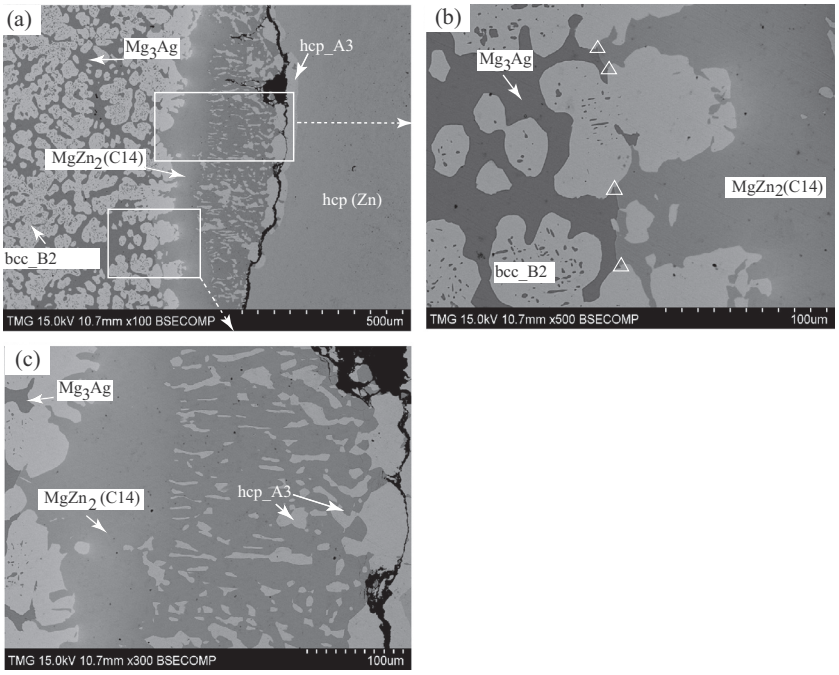

Fig. 4. BSE images of diffusion couple D3.

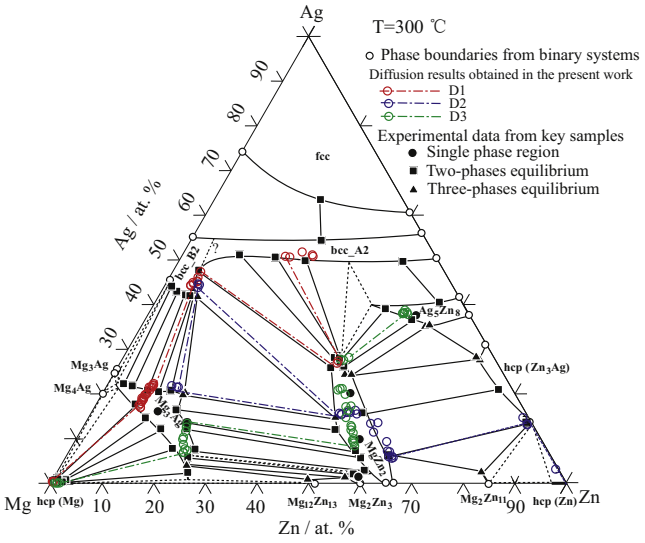

Fig. 5. Isothermal section of Mg–Zn–Ag ternary at 300 °C with experimental data obtained from key samples.

Mg atoms. The solid solubility of Zn and Ag in the hcp (Mg) phase is very limited, less than 0.5 and 0.3 at.%, respectively. The equilibria compositions obtained from the diffusion couple D1, are listed in Table 2.

Fig. 3 shows the BSE images of the diffusion couple D2. Four diffusion layers Ag_5Zn_8, $MgZn_2$ (C14), Mg_3Ag and hcp (Mg) were observed (see Fig. 3a). Furthermore, the two-phase equilibrated microstructure Ag_5Zn_8 + $MgZn_2$ (C14) formed in the end-member of Mg10Zn50Ag40, as shown in Fig. 3b. The EDS line-scan was used to determine the composition profile of phases formed as shown in Fig. 3c. Solid solubilities of 49–56 at.% Zn and 8–17 at.% Ag in the $MgZn_2$ (C14) were observed. The Mg_2Zn (C14) phase formed principally based on the substitutional solution where Zn and Ag atom replaced each other, with a nearly constant Mg at 35 at.%. In contrast to D1, solid solubility of Mg_3Ag formed in D2 with substitution among Ag, Mg, and Zn atoms, as shown in Fig. 3c. Its complex homogeneity range was determined to be 68–71 Mg, 20–23 Zn, and 6–12 Ag in D2 (at.%). In addition, the maximum solid solubility of Ag in the $MgZn_2$ (C14) phase was determined to be 25.7 at.% Ag. Equilibrium compositions of the constituted phases, obtained from the diffusion couple D2, are listed in Table 2. The sequence of the diffusion path in the D2 could be illustrated as: $Ag_5Zn_8 \leftrightarrow MgZn_2$ (C14) $\leftrightarrow Mg_3Ag \leftrightarrow$ hcp (Mg).

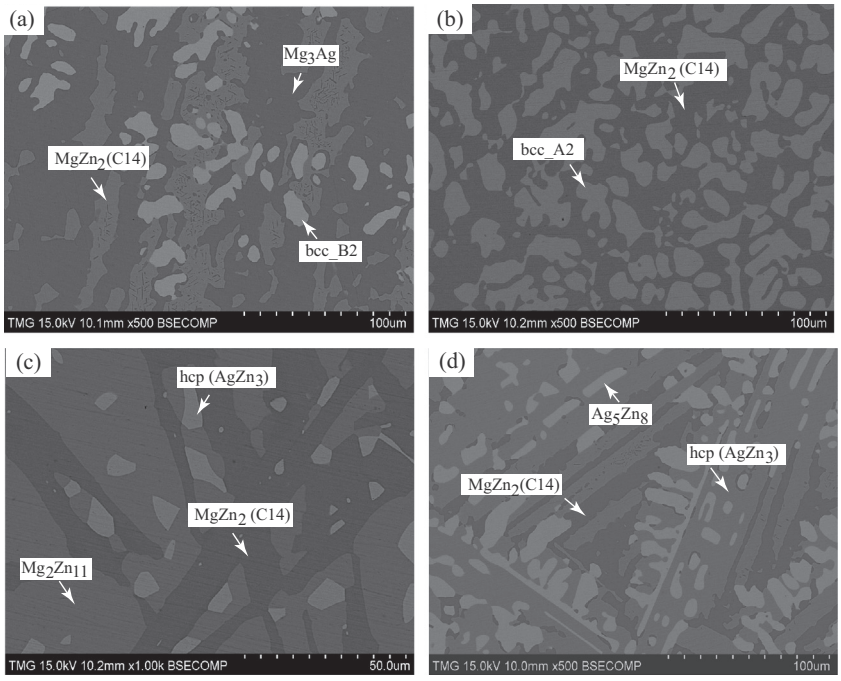

Fig. 6. The BSE images obtained from key samples: (a) A6 (Mg55Zn25Ag20), (b) A13 (Mg30Zn35Ag35), (c) A14 (Mg20Zn75Ag5), (d) A30 (Mg20Zn55Ag25).

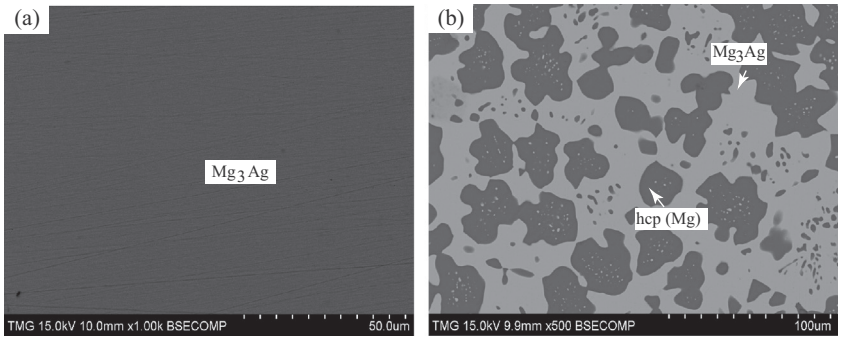

Fig. 7. The BSE images obtained from key samples: (a) A22 (Mg70Zn14Ag16), (b) A16 (Mg80Zn15Ag5).

The BSE images of diffusion couple D3 are shown in Fig. 4. The two-phase equilibrated microstructure Mg_3Ag + bcc_B2 was observed in the end-member of Mg55Zn10Ag35. Four diffusion layers formed in D3. Fig. 4b shows the magnified three-phase equilibrated microstructure of Mg_3Ag + bcc_B2 + $MgZn_2$ (C14) formed on the boundary between end-member (Mg55Zn10Ag35) and the $MgZn_2$ (C14) layer. The equilibrated compositions of each phase of Mg_3Ag, bcc_B2, and $MgZn_2$ (C14) for three phase equilibrium were measured at the position where all three phases existed (marked as triangles in Fig. 4b). The diffusion path passed to a two-phase region of $MgZn_2$ and hcp ($AgZn_3$). Along the diffusion layer, toward the end member Zn, the solid solution of $MgZn_2$ changed, and more Mg was substituted by Zn. The sequence of the diffusion path in the D3 couple could be explicated as: Mg_3Ag + bcc_B2 + $MgZn_2$ (C14) ↔ $MgZn_2$ (C14) ↔ $MgZn_2$ + hcp ($AgZn_3$) ↔ hcp ($AgZn_3$) ↔ Zn. The compositions of the constituted phases obtained in diffusion couple D3 are listed in Table 2. The diffusion paths obtained from D1, D2 and D3 in the present work are shown in Fig. 5. It is found that both the Mg_3Ag and $MgZn_2$ (C14) binary compounds have wide homogeneity ranges extending into ternary system, as shown in Fig. 5. More accurate solubilities were confirmed further and measured using the following key alloys.

3.2. Key samples results

Based on the phase relationships obtained from diffusion couples D1–D3, 35 key alloys (A1–A35) were selected and prepared

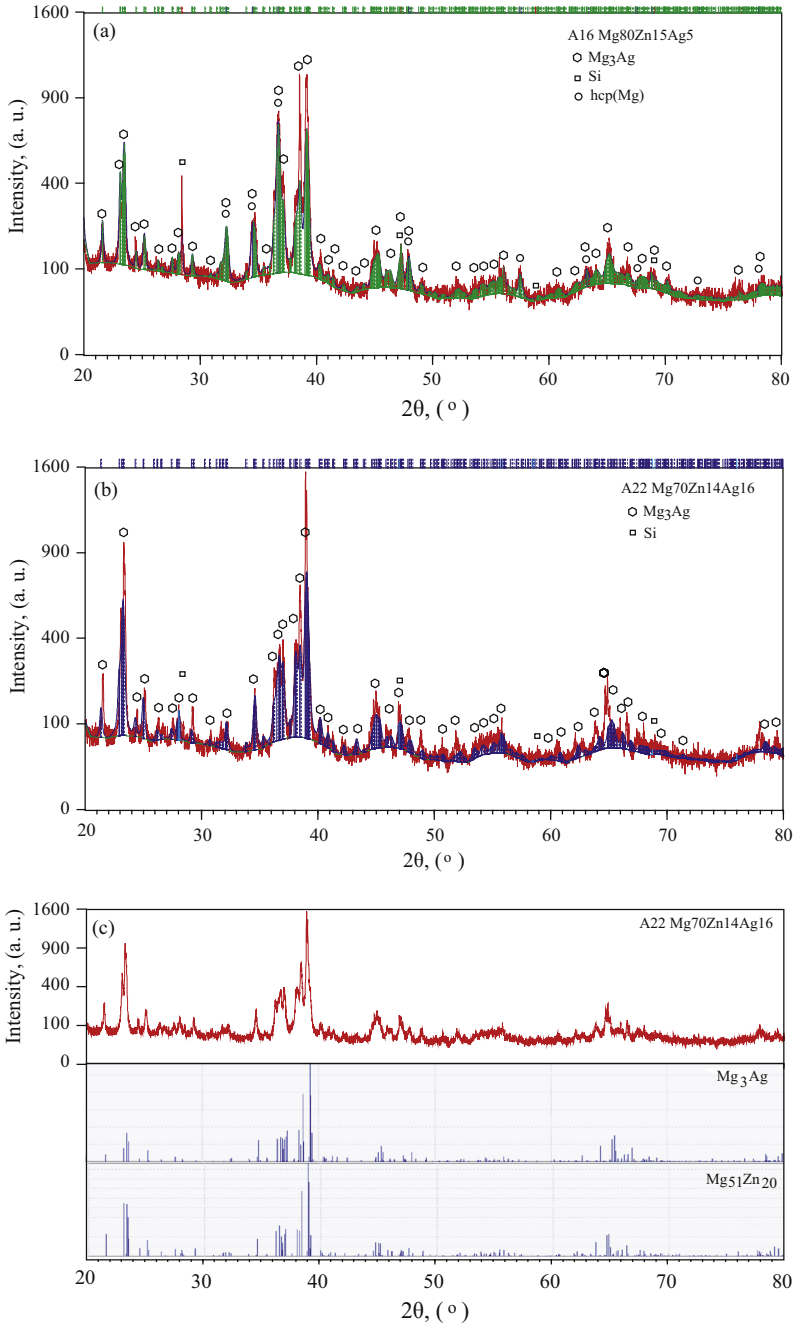

Fig. 8. XRD patterns and refinement results of the representative alloys: (a) A16 (Mg80Zn15Ag5), (b) A22 (Mg70Zn14Ag16), and (c) comparison among of XRD patterns obtained from A22 sample, Mg_3Ag and $Mg_{51}Zn_{20}$ phases.

in order to confirm the phase relationships, and to construct an isothermal section of the Mg–Zn–Ag ternary system at 300 °C.

The three-phase equilibrium Mg_3Ag + bcc_B2 + $MgZn_2$ (C14) observed from diffusion couple D3, was confirmed by key samples A6 and A9. The BSE images obtained from key sample A6 are shown in Fig. 6a. Compositions of the three phases determined from samples A6 are in reasonable agreement with the results obtained from diffusion couple D3. A two-phase equilibrium of bcc_A2 + $MgZn_2$ (C14) was observed in the key sample A13, as shown in Fig. 6b. The three-phase field of $MgZn_2$ + Mg_2Zn_{11} + hcp ($AgZn_3$) was observed in key sample A14 as shown in Fig. 6c. According to the present EDS analysis of sample A14, the maximum solid solubility of Ag in Mg_2Zn_{11} was found to be 2.7 at.%. From the key samples A30 and A31, the three-phase equilibrium of hcp ($AgZn_3$) + Ag_5Zn_8 + $MgZn_2$ was observed. The BSE image of key sample A30 is shown in Fig. 6d. The maximum solid solubility of Mg in Ag_5Zn_8 compound was found to be 9.7 at.%.

In addition, the ternary extended solid solubility of Mg_3Ag was confirmed with XRD analysis on samples A16 and A22. The BSE images obtained from these two samples are shown in Fig. 7. A single phase microstructure was obtained in sample A22 (see Fig. 7a), and a two-phase field of hcp (Mg) + Mg_3Ag was obtained in sample A16 (see Fig 7b). The Rietveld analysis of samples A16 and A22 shows that both samples contain the Mg_3Ag (cF264) phase, as shown in Fig. 8, which confirms the previous findings obtained by SEM. The XRD refinement results, shown in Fig. 8a and b, indicate the presence of solid solution of Mg_3Ag. The Mg_3Ag phase was also found in key alloys A1–A7, A16–A18, and A21–A27. The EDS measurements of these key alloys show that solid solubility of Mg_3Ag occurred by the substitution of Ag, Mg, and Zn. The SEM and XRD results for Mg_3Ag, obtained from the key alloy, are in good agreement with the results observed in diffusion couples (D1–D3). Furthermore, after comparison with the XRD patterns of $Mg_{51}Zn_{20}$ from Higashi et al. [37], shown in Fig. 8c, it is clearly revealed that there are the same dominating peaks (at 2θ of 23°, 37–40°, and 65°), with minor shifts between $Mg_{51}Zn_{20}$ and Mg_3Ag. The Rietveld analysis results indicate that $Mg_{51}Zn_{20}$ and Mg_3Ag may have the same crystal structure. But the verification on the crystal structures of $Mg_{51}Zn_{20}$ and Mg_3Ag is still needed due to the two different crystal types previous reported [24,37]. The solid solubility of Mg_3Ag close to the $Mg_{51}Zn_{20}$ compound in the Mg–Zn binary side, may lead to the conclusion that a continuous homogeneity range between the Mg_3Ag and $Mg_{51}Zn_{20}$ compounds can form in the temperature range 325–342 °C, where $Mg_{51}Zn_{20}$ is stable in the Mg–Zn binary system [22]. This proposal also requires a further experiment.

Furthermore, $MgZn_2$ (C14) also extends into the Mg–Zn–Ag ternary system with a maximum solubility of 28.7 at.% Ag at 300 °C. A large continuous bcc solid solution phase, encompassing between MgAg (bcc_B2) and AgZn (bcc_A2), was also found in key samples A6–A9, A12, A13, A24–A27, A33 and A35. Measurements on the order–disorder phase transformation (B2/A2) boundary of the bcc phase in the Ag-rich region were not carried out in the present work. This is because our present phase equilibrium measurements were mainly focused on the Mg-rich region, for Mg-based alloy applications. The phase equilibria obtained using equilibrated key samples are shown in Fig. 5. All the compositions of the constituent phases of the equilibrated key samples were analyzed by EDS and are listed in Table 3. The phase equilibria relationships and compositions, obtained using equilibrated key alloys and diffusion couple techniques, are in good agreement.

3.3. Isothermal section

The phase equilibria obtained using equilibrated key samples and diffusion couples are shown in Fig. 9. Four three-phase fields: hcp ($AgZn_3$) + Ag_5Zn_8 + $MgZn_2$, Mg_3Ag + $Mg_{12}Zn_{13}$ + Mg_2Zn_3, Mg_3Ag + bcc_B2 + $MgZn_2$, and $MgZn_2$ + Mg_2Zn_{11} + hcp ($AgZn_3$) have been determined using key alloys and diffusion couples. Five undetermined three-phase fields: Mg_4Ag + Mg_3Ag + Mg, Mg_3Ag + hcp (Mg) + $Mg_{12}Zn_{13}$, Mg_3Ag + $MgZn_2$ + Mg_2Zn_3, Ag_5Zn + bcc_A2 + $MgZn_2$, and Mg_2Zn_{11} + hcp(Zn) + hcp ($AgZn_3$), are drawn with dashed lines. The maximum solid solubility of Ag in the hcp (Mg) phase was found to be less than 0.5 at.%. A large extended solid solubility of the Mg_3Ag phase was measured in the present work with key samples and diffusion couples, and confirmed by XRD. The solid solubility of Ag in the $Mg_{12}Zn_{13}$ phase was determined to be 1.1 at.%. The solid solubility of Ag in Mg_2Zn_3 was estimated to be less than 4 at.%, based on the equilibria information of the $MgZn_2$ and Mg_3Ag obtained in the present work. A large extended solid solubility of the $MgZn_2$ phase was measured, and the maximum solid solubility of Ag in $MgZn_2$ was determined to be 28.7 at.%.

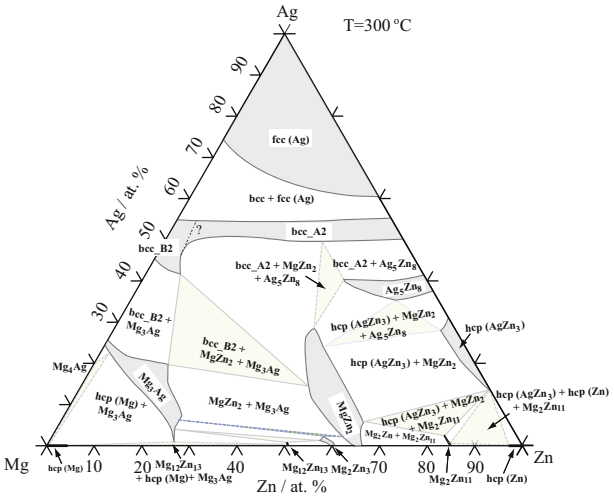

Fig. 9. Isothermal section of Mg–Zn–Ag ternary at 300 °C.

4. Conclusions

The isothermal section of the Mg–Zn–Ag system at 300 °C was investigated using diffusion couple and classical equilibrated alloys techniques. Four three-phase equilibrium regions were found. The isothermal phase diagram for the complete composition region was constructed. The remaining five three-phase equilibrium regions were proposed as: Mg_4Ag + Mg_3Ag + Mg, Mg_3Ag + hcp (Mg) + $Mg_{12}Zn_{13}$, Mg_3Ag + $MgZn_2$ + Mg_2Zn_3, Ag_5Zn + bcc_A2 + $MgZn_2$, Mg_2Zn_{11} + hcp(Zn) + hcp ($AgZn_3$). It was found that Mg_3Ag and $MgZn_2$ extend into the Mg–Zn–Ag ternary system with significant homogeneity ranges. The extended solid solubilities of the other binary compounds: $Mg_{12}Zn_{13}$, Mg_2Zn_3, Mg_2Zn_{11}, Ag_5Zn_8 and hcp ($AgZn_3$), were also determined in the ternary system. In addition, the bcc solid solution existing in the Mg–Ag and Ag–Zn binary systems also forms a continuous solid solution in the Mg–Zn–Ag ternary system at 300 °C.

Acknowledgements

Financial support from General Motors of Canada Ltd. and the Natural Sciences and Engineering Research Council of Canada through the CRD grant program is gratefully acknowledged. The support in the experimental part from Mr. Tian Wang, Mr. Xin Zhang, and Dr. Dmytro Kevorkov from Concordia University is acknowledged by the authors.

References

[1] G. Ben-Hamu, D. Elizer, A. Kaya, Y.G. Na, K.S. Shin, Microstructure and corrosion behavior of Mg–Zn–Ag alloys, Mater. Sci. Eng. A 435–436 (2006) 579–587.

[2] C.L. Mendis, K. Oh-ishi, K. Hono, Enhanced age hardening in a Mg–2.4 at. % Zn alloy by trace additions of Ag and Ca, Scripta Mater. 57 (2007) 485–488.

[3] C.L. Mendis, K. Oh-ishi, Y. Kawamura, T. Honma, S. Kamado, K. Hono, Precipitation-hardenable Mg–2.4Zn–0.1Ag–0.1Ca–0.16Zr (at. %) wrought magnesium alloy, Acta Mater. 57 (2009) 749–760.

[4] T. Bhattacharjee, C.L. Mendis, K. Oh-ishi, T. Ohkubo, K. Hono, The effect of Ag and Ca additions on the age hardening response of Mg–Zn alloys, Mater. Sci. Eng. A 575 (2013) 231–240.

[5] S.C. Park, J.D. Lim, D. Eliezer, K.S. Shin, Microstructure and mechanical properties of Mg–Zn–Ag Alloys, Mater. Sci. Forum 419–422 (2003) 159–164.

[6] P. Ghosh, M.D. Mezbahul-Islam, M. Medraj, Critical assessment and thermodynamic modeling of Mg–Zn, Mg–Sn, Sn–Zn and Mg–Sn–Zn system, Calphad 36 (2012) 28–43.

[7] F. Meng, J. Wang, L. Liu, Z. Jin, Thermodynamic modeling of the Mg–Sn–Zn ternary system, J. Alloys Comp. 508 (2010) 570–581.

[8] J. Wang, P. Hudon, D. Kevorkov, P. Chartrand, I.-H. Jung, M. Medraj, Experimental and thermodynamic study of the Mg–Sn–In–Zn quaternary system, J. Alloys Comp. 588 (2014) 75–95.

[9] R. Agarwal, S.G. Fries, H.L. Lukas, G. Petzow, F. Sommer, T.G. Chart, G. Effenberg, The Mg–Zn system, Z. Metallkd. 83 (1992) 216–223.

[10] J. Wang, P. Hudon, D. Kevorkov, P. Chartrand, I.-H. Jung, M. Medraj, Thermodynamic and experimental study of the Mg–Sn–Ag–In quaternary system, J. Phase Equilib. Diffr. 35 (2014) 284–313.

[11] V.E. Kolesnichenko, V.V. Karonik, S.N. Tsyganova, T.A. Kupriyanova, L.N. Sysoeva, Phase equilibria in the Mg–Ag system in the eta phase region, Izv. Akad. Nauk SSSR Neorg. Mater 5 (1988) 186–191.

[12] M. Lim, J.E. Tibballs, P.L. Rossiter, Thermodynamic assessment of Ag–Mg binary system, Z. Metalld. 88 (1997) 160–167.

[13] A.A. Nayeb-Hashemi, J.B. Clark, The Ag–Mg system, Bull. Alloy Phase Diagr. 5 (1984) 348–354.

[14] J. Wang, P. Chartrand, I.-H. Jung, Thermodynamic description of the Ag–(Ca, Li, Zn) and Ca–(In, Li) binary systems, Calphad (2015). accepted for publication.

[15] T. Gomez-Acebo, Thermodynamic assessment of the Ag–Zn system, Calphad 22 (1998) 203–220.

[16] K.W. Andrews, H.E. Davies, W. Hume-Rothery, C.R. Oswin, The equilibrium diagram of the system silver–zinc, Proc. Roy. Soc. A177 (1941) 149–167.

[17] G.I. Petrenko, Over zinc silver alloys, Z. Anorg. Allg. Chem. 48 (1906) 347–363.

[18] G.J. Petrenko, B.G. Petrenko, Zur Frage des Aufbaus der γ-phase in den Legierungen Ag–Zn, Z. Anorg. Allg. Chem. 185 (1930) 96–100.

[19] E.A. Owen, I.G. Edmunds, The determination of certain phase boundaries in the silver–zinc thermal diagram by X-ray analysis, J. Inst. Met. 57 (1935) 297–306.

[20] E.A. Owen, I.G. Edmunds, X-ray study of silver–zinc alloys rich in silver above the beta-transformation temperature, J. Inst. Met. 62 (1938) 266–278.

[21] E.A. Owen, I.G. Edmunds, Silver–zinc equilibrium diagram and the structure of the beta phase, J. Inst. Met. 63 (1938) 291–301.

[22] J. Clark, F. Rhines, Central region of the Mg–Zn phase diagram, Trans. Am. Inst. Min. Metall. Eng. 209 (1957) 425–430.

[23] M.V. Prokofev, V.E. Kolesnichenko, V.V. Karonik, Mg–Ag system, Izv. Akad. Nauk SSSR Neorg. Mater. 21 (1985) 1332–1334.

[24] G. Kreiner, S. Spiekermann, Crystal structure of ϵ $Ag_{7+x}Mg_{26-x}$-A binary alloy phase of the mackay cluster type, Z. Anorg. Allg. Chem. 627 (2001) 2460–2468.

[25] C.T. Heycock, F.H. Neville, The freezing points of alloys containing zinc and another metal, J. Chem. Soc. 71 (1896) 383–422.

[26] G.V. Raynor, R.A. Smith, The constitution of the silver-rich Ag–Mg–Zn alloys, J. Inst. Met. 76 (1949) 389–406.

[27] Y. Matsuo, S. Minamigawa, K. Katada, Phase relation and superlattice formation in the silver–zinc–magnesium (AgZn–AgMg) quasibinary alloys, Acta Metall. 25 (1977) 1179–1186.

[28] Y. Matsuo, K. Katada, Phase relation in the ternary alloy silver–magnesium–zinc (AgMgZn), J. Phys. Soc. Jpn. 38 (1975) 281.

[29] J. Wang, N. Miao, P. Chartrand, I.-H. Jung, Thermodynamic evaluation and optimization of the (Na + X) binary systems (X= Ag, Ca, In, Sn, Zn) using combined Calphad and first-principles methods of calculation, J. Chem. Thermodyn. 66 (2013) 22–33.

[30] J. Wang, J. Han, I.-H. Jung, D. Bairos, P. Chartrand, Thermodynamic optimizations on the binary Li–Sn system and ternary Mg–Sn–Li system, Calphad 47 (2014) 100–113.

[31] Y.N. Zhang, X.D. Liu, Z. Altounian, M. Medraj, Coherent nano-scale ternary precipitates in crystallized Ca4Mg72Zn24 metallic glass, Scripta Mater. 68 (2013) 647–650.

[32] Y.N. Zhang, G.J. Rocher, B. Briccoli, D. Kevorkov, X.B. Liu, Z. Altounian, M. Medraj, Crystallization characteristics of the Mg-rich metallic glasses in the Ca–Mg–Zn system, J. Alloys Comp. 552 (2013) 88–97.

[33] Y.N. Zhang, D. Kevorkov, X.D. Liu, F. Bridier, P. Chartrand, M. Medraj, Homogeneity range and crystal structure of the $Ca_2Mg_5Zn_{13}$ compound, J. Alloys Comp. 523 (2012) 75–82.

[34] Y.N. Zhang, D. Kevorkov, F. Bridier, M. Medraj, Experimental investigation of the Ca–Mg–Zn system using diffusion couples and key alloys, J. Sci. Tech. Adv. Mater. 12 (8) (2011) 025003.

[35] Y.N. Zhang, D. Kevorkov, J. Li, E. Essadiqi, M. Medraj, Determination of the solubility range and crystal structure of the Mg-rich ternary compound in the Ca–Mg–Zn system, Intermetallics 18 (12) (2010) 2402–2411.

[36] P. Villars, K. Cenzual, Pearson's Crystal Data, Crystal Structure Database for Inorganic Compounds, ASM International, Materials Park (OH), 2007.

[37] I. Higashi, N. Shiotani, M. Uda, T. Mizoguchi, H. Katoh, The crystal structure of $Mg_{51}Zn_{20}$, J. Solid State Chem. 36 (1981) 225–233.